Drag and near wake characteristics of flat plates normal to the flow with fractal edge geometries

J. Nedić[1], B. Ganapathisubramani[2] and J. C. Vassilicos[1]

[1]Turbulence, Mixing and Flow Control Group, Department of Aeronautics, Imperial College London, London SW7 2AZ, UNITED KINGDOM
[2]Aerodynamics and Flight Mechanics Research Group, University of Southampton, Southampton SO17 1BJ, UNITED KINGDOM

E-mail: jovan.nedic@imperial.ac.uk; g.bharath@soton.ac.uk; j.c.vassilicos@imperial.ac.uk

Abstract. Past results have suggested that the coefficient of drag and shedding frequencies of regular polygon plates all fall within a very narrow band of values. In this study, we introduce a variety of length-scales into the perimeter of a square plate and study the effects this has on the wake characteristics and overall drag. The perimeter of the plate can be made as long as allowed by practical constraints with as many length-scales as desired under these constraints without changing the area of the plate. A total of eight fractal-perimeter plates were developed, split into two families of different fractal dimension all of which had the same frontal area. It is found that by increasing the number of fractal iterations, thus the perimeter, the drag coefficient increases by up to 7%. For the family of fractal plates with the higher dimension, it is also found that when the perimeter increases above a certain threshold the drag coefficient drops back again. Furthermore, the shedding frequency remains the same but the intensity of the shedding decreases with increasing fractal dimension. The size of the wake also decreases with increasing fractal dimension and has some dependence on iteration without changing the area of the plate.

Keywords: Fractal Geometries, Flat Plates, Wakes, Drag

1. Introduction

The flow around regular polygon plates have been studied numerous times in the past, the most common of which has been the axisymmetric circular disk, however several studies have also focused their attention on square plates. This is not to say that other shapes have not also been considered, which is why we provide a brief overview of the numerous studies that have been done on regular polygon plates which show that the drag and shedding properties of the wake generated by these plates all fall within a very narrow band of values, as shown in figure 1.

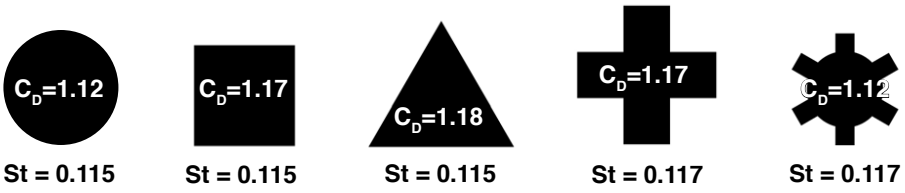

Figure 1. The drag coefficient and Strouhal number for a variety of shapes, data taken from Fail et al. [1] except for the cross which is taken from this study. The Strouhal number is $St = (f\sqrt{A})/U_\infty$ where f is the shedding frequency, A the area of the plate and U_∞ the velocity of the incoming flow.

1.1. Circular and Square Disks

Since the first basic flow visualisations of the wake structure behind a circular disk were done by Marshall & Stanton [2], researchers have focused on understanding this flow in more detail. To the authors knowledge, Fail et al. [1], obtained some of the earliest measurements of the drag and shedding frequencies of circular disks as well as other plates of similar frontal area. For the circular disk, they found that the drag coefficient was 1.12 whilst the Strouhal number, St, based on the square root of the frontal area, was found to be 0.115. Carmody [3] took hot-wire and pressure measurements behind a circular disk showing that 95% of the total transfer of energy from the mean motion to the turbulent motion takes place very close to the plate, usually within the first three plate diameters. Carmody [3] also offered a C_D of 1.14.

Thus far, the characteristics of the plates had only been considered with a laminar freestream. However, in 1971 Bearman [4] began looking at the effect that a turbulent freestream has on the drag force on plates. Bearman [4] studied square and circular disks of varying size and found the base pressure coefficient, $(C_P)_b$ to be -0.363, and that it was the same for both types of plates. With the addition of a turbulent freestream, the base pressure decreased and with it, the drag coefficient increased. The eight inch square plate, for example, had a C_D of 1.152 with a laminar freestream, but this then increased with a turbulent freestream typically by a few percent.

The influence of a turbulent freestream on the drag of plates was further studied by Humphries and Vincent ([5], [6]) who found that the drag of a circular disk could be increased up to 1.28 as the turbulent intensity and integral length scale in the turbulent freestream were increased. These studies, as well as the one by Bearman [4] suggested that the reason for the increase in drag was due to a delay of the shear layer's transition to turbulence which would keep the base pressure low and hence increase the drag.

Some further progress in the understanding of the wake structure was made by Berger et al. [7], whose experiments focused on the near wake at relatively low Reynolds numbers and revealed various regimes with various associated shedding frequencies. Further studies by Lee and Bearman [8], Miau et al [9], Kiya et al [10] and Shenoy and Kleinstreuer [11] have added to the understanding of the wake of a circular disk, however, as quoted by Kiya et al[10]: "the wake of a square plate normal to the flow is not understood yet."

1.2. Other Polygon Shaped Disks

Although the study of regular polygon plates has been dominated by circular disks as well as square plates, a few other shapes have also been considered. Fail et al [1], as well as studying these two plates, also studied an equilateral triangle plate and a tabbed plate - all four plates used by Fail et al [1] are shown, scaled, in figure 4(k-n). What was rather surprising was that all of these plates had similar drag coefficients between 1.12 and 1.15 and Strouhal numbers between 0.115 and 0.117 when the incoming flow was laminar. A similar C_D value of 1.18 was found by Humphries and Vincent [6] for the triangular plate with a laminar freestream.

Elliptical and rectangular plates were studied by Kiya and Abe [12] and again by Kiya et al [10] where the main finding was that the wake had the same shape as the plate itself, however, the alignment is rotated by 90° with the major axis of the plate aligned with the minor axis of the wake. Two distinct shedding frequencies are also observed, one for each axis, however the Strouhal number is found to decrease with aspect ratio of the plate, from roughly 0.12 where the aspect ratio is 1, to roughly 0.06 for the major axis and 0.11 for the minor axis of an elliptical plate with an aspect ratio of 3.

1.3. Large scale or small scale effects?

From the literature it is clear that both the drag coefficient and the Strouhal number of circular disks and regular polygon plates appear to fall within a very narrow band of values, with the difference between their C_D values being at most, no more than 5%. Even the tabbed plate, which could have three defined length-scales: one associated with the inner diameter, one with the outer diameter i.e. including the tabs, and the tab itself, has a similar C_D and St. This plate is of particular interest as one would expect the tabs to somehow interact with the shear layer that may change its transition point and with it the drag coefficient, as suggested by the arguments of Bearman [4] and Humphries and Vincent [6][5]. This, however, is not the case as Fail [1] shows that

the circular plate and the tabbed plate have the same value of $C_D = 1.12$. The question then becomes what if more length-scales were introduced, could that cause a change that would create a larger drag coefficient?

If an energy balance is done between the work required to move a plate through a fluid in the direction normal to its plane, and the dissipation of the turbulent kinetic energy that is produced in the fluid (see Appendix), then the following expression can be obtained:

$$C_D = C_V C_{\bar{\epsilon}} \tag{1}$$

where the wake volume coefficient is defined as $C_V = V_{wake}/2A^{1.5}$, V_{wake} being the volume filled by the wake, A the frontal area of the plate and $C_{\bar{\epsilon}}$ is the coefficient of the average rate of dissipation of turbulent kinetic energy in the volume of the wake, as defined by equation 2.

$$\bar{\epsilon} = (C_{\bar{\epsilon}} U_\infty^3)/\sqrt{A} \tag{2}$$

It is now apparent with (1) that the drag of a blunt object can be controlled by either changing the dissipation in the wake, or by keeping the dissipation constant but somehow changing the size of the wake or even a combination of the two. This also poses the question whether the volume of the wake can be changed without changing the area of the plate. Here we show that it is possible to achieve this, thus manipulating the drag, by introducing a range of length-scales on the edge of the plate without changing the area. The purpose of this study is to investigate these phenomena. We use fractal geometries to introduce a variety of length-scales to the edge of a square plate. In doing so we follow recent works by e.g. Seoud & Vassilicos [13], Laizet & Vassilicos [14] and Kang et al. [15] amongst others (see exhaustive list of references in Gomes-Fernandes et al.[16]). In particular, Kang et al.[15] measured drag forces of Sierpinski carpets and triangles, similar to the shapes used by Aly et al [17] and Nicolleau et al [18] who investigated the pressure drop across fractal shaped orifices. Laizet & Vassilicos [14] showed that the pressure drop across a space-filling ($D_f = 2$) fractal square grid is much lower than across a regular grid with same blockage and same effective mesh size.

2. Experimental set-up

Over the course of this study, two wind tunnels were used. The 'Honda' Wind Tunnel in the Department of Aeronautics at Imperial College London has a working cross-section of 5ft x 10ft, a length of 30ft and a top speed of $40ms^{-1}$. The second tunnel was the 'Donald Campbell' (DC) Tunnel, again at Imperial College London, which has a working cross-section of 4ft x 5ft (1.22m x 1.52m), a length of 11ft (3.35m) and a top speed of $40ms^{-1}$. The blockage ratio i.e. ratio between the frontal area of the plate to the cross-sectional area of the test section was found to be 1.41% in the 'Honda' tunnel, whilst it was 3.53% in the DC Tunnel. Background turbulence levels in the Honda and DC Tunnel were found to be 0.3% and 0.23% respectively.

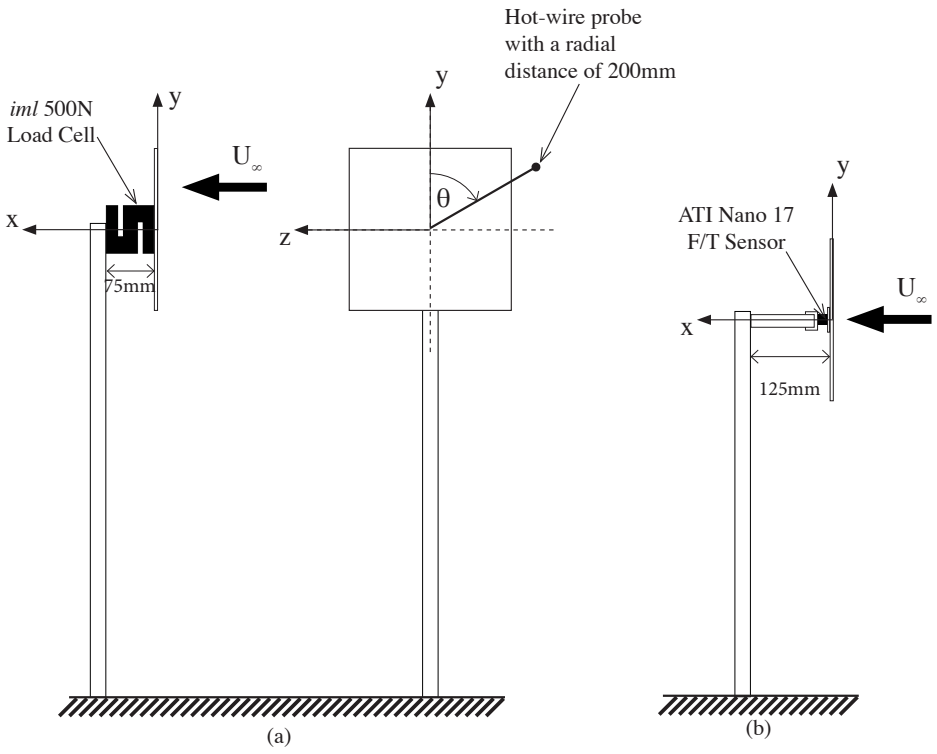

Figure 2. Schematic of the experimental set-up in (a) the Honda Wind Tunnel with both side and front view, and (b) the side on view in the Donald Campbell Tunnel.

The basic set-up in both tunnels included a stand with a protruding arm onto which the plates were mounted. For the Honda measurements, this extrusion was an *iml* Z type 500N load cell which has a total inaccuracy of $< \pm 0.05\%$ of full-scale range, whilst in the DC Tunnel, the *iml* sensor was used as well as a more accurate six-axis, ATI Nano17 Force/Torque Sensor, which was attached on the end of a 100mm steed rod - see figure 2b. This sensor has a range of 35N in the direction of the drag force and a resolution of 1/160 N, but is also capable of measuring the moments about three axes with a resolution of 1/32 Nmm. In the DC Tunnel, force/torque measurements were taken for a range of free-stream velocities, U_∞, from $5ms^{-1}$ to $20ms^{-1}$ in $2.5ms^{-1}$ intervals, with data sampled for 60 seconds which was satisfactory for converged statistics of the mean and fluctuating values. A single set of measurement at $U_\infty = 20ms^{-1}$ were taken in the Honda Tunnel.

Hot-wire and pressure measurements were taken downstream of the plates. A rake of Pitot tubes, in a 2x10 matrix spanning a distance of 450mm and a spacing of 50mm was placed on the traverse in the DC Tunnel. The rake was then traversed vertically in the y-direction to get a 2D plane of measurements, creating a 10x10 matrix of data points, covering a distance of 450mm in both directions and a spacing of 50mm between successive points. This spacing gave a ratio between probe diameter to probe spacing of 10, which was deemed to be sufficient to avoid interference effects. Measurements of the

pressure were taken for a series of downstream locations from two to eight characteristic lengths, which is defined as the square root of the frontal area of the plates. The Pitot tubes were connected to a 32 channel Chell Pressure Transducer, with the static pressure in the tunnel being taken as the reference for all the measurements. The hot-wire probe is made up of a Platinum-Rhodium alloy wire (90-10%) etched to a diameter of 5μm, and is connected to a Dantec Dynamics miniCTA with an overheat ratio set to 1.5.

2.1. Definition of fractal edge geometries

The fractal dimension, D_f is defined mathematically by equation 3 - see Mandelbrot [19] - and measures how rough or smooth an object is. For a line in a 2D plane, a value of one would mean a smooth straight line, whilst any value greater than one would mean a rough shape, the maximum value of D_f being 2. The parameters defining the fractal edges of our plates are in equations 3-6.

$$D_f = \frac{log(d^n)}{log(\frac{\lambda}{l_n})} \tag{3}$$

$$l_n = \lambda / r^n \tag{4}$$

$$r = 4(\cos\alpha - 1) + d \tag{5}$$

$$P_n = S d^n l_n \tag{6}$$

where r is the ratio between successive lengths, P_n is the perimeter of the plate at iteration n and S is the number of sides on the base shape on which the fractal edges are applied ($S = 4$ for a base square plate). A simple way to understand the fractal shape of the edge is illustrated in figure 3. The base straight line of length λ is replaced by a number, d, of segments of length l_1 such that the area under the line remains the same. This is iteration $n = 1$. The second iteration $n = 2$ consists of replacing each individual segment of length l_1 by the same pattern of d segments, but smaller i.e. the segments now have a length $l_2 = l_1/r$. And so on for as many iterations required. A total of eight 'fractal plates' were manufactured, as well as a square and a cross plate. The

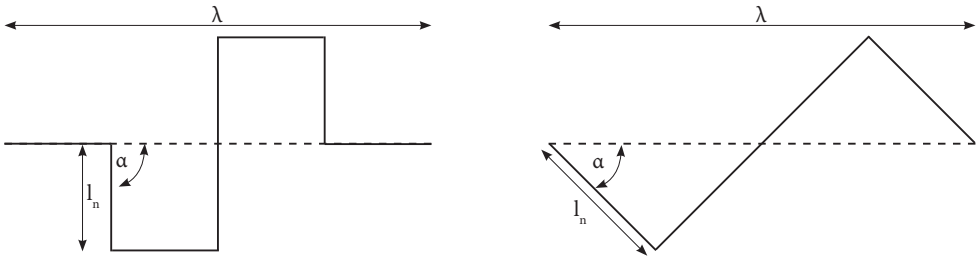

(a) $D_f = 1.5$ (b) $D_f = 1.3$

Figure 3. Illustration of a fractal iteration with corresponding definitions of fractal parameters

Name	D_f	n	P(m)	$l_n(mm)$
Square	1.0	0	1.03	256.20
Cross	1.0	0	1.37	114.58
1.3(1)	1.3	1	1.45	90.58
1.3(2)	1.3	2	2.05	32.03
1.3(3)	1.3	3	2.90	11.32
1.3(4)	1.3	4	4.01	4.00
1.5(1)	1.5	1	2.05	64.05
1.5(2)	1.5	2	4.01	16.01
1.5(3)	1.5	3	8.20	4.00
1.5(4)	1.5	4	16.40	1.00

Table 1. Fractal plate dimensions - D_f is the fractal dimension, n is the iteration of the fractal pattern, P is the perimeter given in metres and l_n is the length of each segment at the given iteration in mm.

fractal plates are based on a square plate of 256mm x 256mm x 5mm in size, 5mm being the thickness of the plate, and were designed such that the area remained constant, achieved by a simple 'add on and take away' method as in the example of figure 3.

Two patterns were used to generate the fractal plates, a square ($\alpha = 90°$, $d = 8$ and $D_f = 1.5$) and a triangle pattern ($\alpha = 45°$, $d = 4$ and $D_f = 1.3$), with the square pattern shown in figure 3. Consecutive iterations were obtained by applying the same pattern to each new length-scale generated, repeated up to four times, giving four plates for each pattern as can be seen in figure 4. It can also be seen from this figure that the fractal plates no longer resemble a square, but more of a cross shape, hence a cross plate was also manufactured. The same figure also has scaled drawings of the plates used by Fail et al [1].

Although all the plates have the same frontal area, the perimeter (P_n) varied as can be seen in table 1, where the perimeter can be anything up to 16 times longer than the original square plate. It is by applying a fractal pattern that we are able to introduce a larger perimeter and varying length-scales into the flow without changing the area of the plate.

3. Force measurements

3.1. The effect of perimeter and fractal dimension

Figure 5 shows the drag coefficient for the plates, collected in the DC tunnel using both types of sensors where we can deduce that the change in drag coefficient is not down to the resolution and accuracy of the *iml* sensor, within acceptable experimental error. Note that the maximum difference between the largest and smallest drag force measurement is 1.57N based on a freestream velocity of $20ms^{-1}$, which is 250 times larger than the resolution of the ATI sensor, which has a resolution of 1/160N. The largest

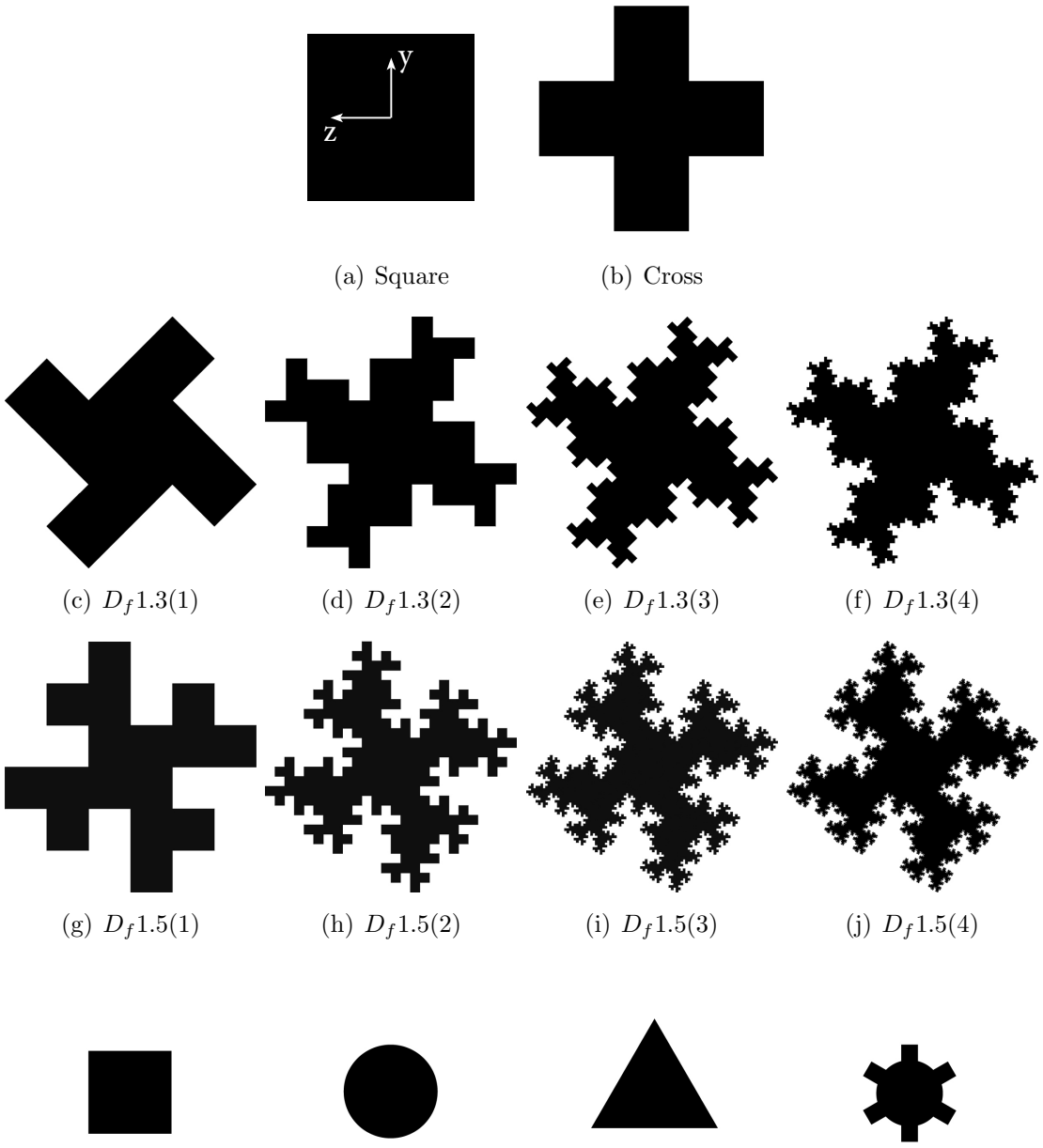

(a) Square (b) Cross

(c) $D_f1.3(1)$ (d) $D_f1.3(2)$ (e) $D_f1.3(3)$ (f) $D_f1.3(4)$

(g) $D_f1.5(1)$ (h) $D_f1.5(2)$ (i) $D_f1.5(3)$ (j) $D_f1.5(4)$

(k) Square used by [1] (l) Circle used by [1] (m) Triangle used by [1] (n) Tabbed used by [1]

Figure 4. Scaled drawings of flat plates used in this experiment, as well as those by Fail [1]. The frontal area for diagrams (a) to (j) are identical. Note that the plates were mounted in the tunnel with the orientation shown above, with the vertical and spanwise axis shown in figure 4(a)

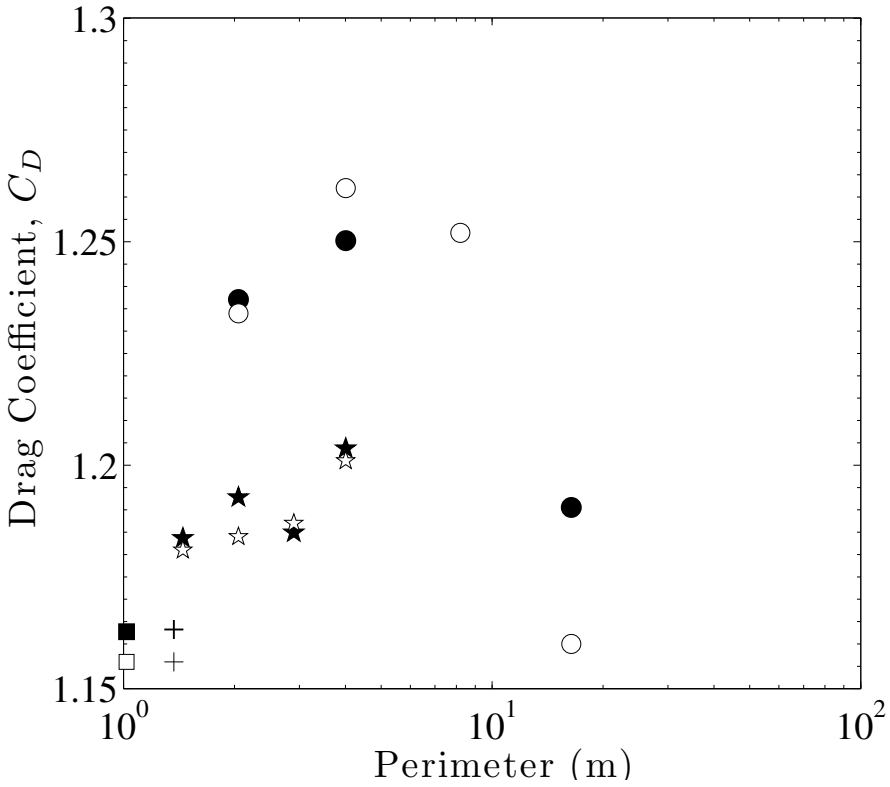

Figure 5. Change in drag coefficient with perimeter for the square plate (□), cross plate (+), D_f=1.3 series of plates (⋆) and D_f = 1.5 series of plates(∘).Open shapes refer to measurements taken with the iml sensor and solid shapes refer to measurements taken with the ATI sensor, both in the DC tunnel. There are also two measurements for the cross plate, one for each sensor.

discrepancy between the two sensors is obtained for the $D_f = 1.5(4)$ plate for which we have no definite explanation for the time being, however despite this discrepancy between the two sensors, conclusions can already be made from this one figure. Firstly, there is a clear effect of iteration within each fractal dimension which is seen in figure 5 as an increase with increasing perimeter length, and there is an effect of fractal dimension itself. For the $D_f = 1.3$ family of plates, it is only at the last iteration that we see a noticeable increase in C_D compared to the square plate of roughly 3.5%, which is similar to the maximum difference between all the plates in figure 1. As the fractal dimension is increased, a more pronounced change in C_D is observed, with the $D_f = 1.5(2)$ plate showing the biggest increase in C_D, roughly 7%. This particular plate can also be compared to the $D_f = 1.3(4)$ plate as both sets of plates have the same perimeter and thus shows that by increasing the fractal dimension, one can increase the drag of the plate irrespective of perimeter length and frontal area, implying that the fractal dimension is a controlling factor in the drag of these plates. The same can be said for the $D_f = 1.3(2)$ and the $D_f = 1.5(1)$ plates, which also have the same perimeter - see table 1. Special note must also be taken of the cross plate in figure 5, which has the same

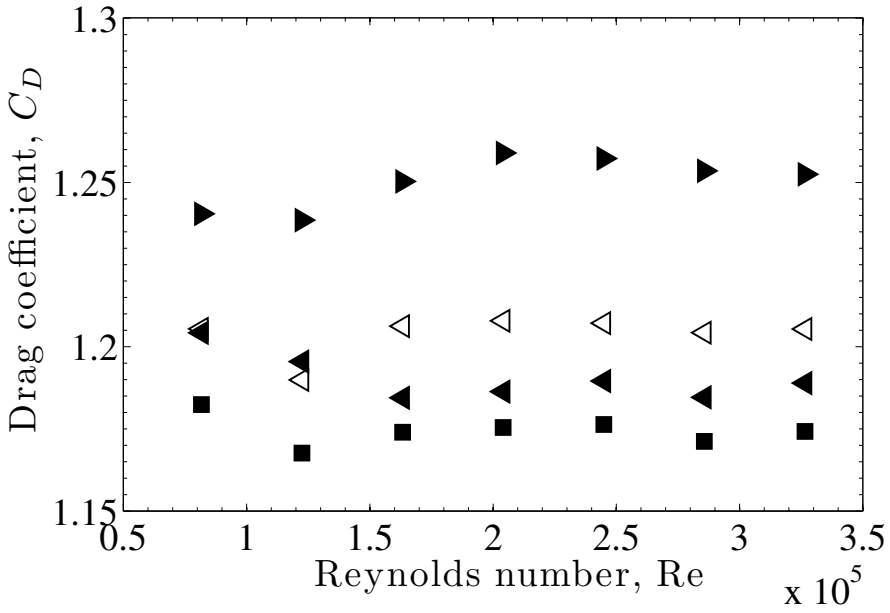

Figure 6. Variation of the drag coefficient, C_D, with Reynolds number for the square plate (■), $D_f = 1.3(4)$ plate (◁), $D_f = 1.5(2)$ plate (▶) and the $D_f = 1.5(4)$ plate (◀). Data taken from the Donald Campbell tunnel using the ATI Nano 17 sensor

drag coefficient as the square plate, adding to the evidence that the drag coefficient of non-fractal plates do fall within a narrow band of values.

Of particular interest in figure 5 is the last iteration of the $D_f = 1.5$ family of plates, where a sharp decline in C_D is observed. Hence, two issues must be addressed with respect to the $D_f = 1.5$ family of plates: the initial increase in C_D with fractal iteration, and the sudden drop of C_D as the iteration increases past a certain value.

3.2. The effect of Reynolds Number

Equation (1) shows that the coefficient of drag is independent of Reynolds number, $Re = U_\infty\sqrt{A}/\nu$, as $Re \to \infty$ if in this limit $C_{\bar{\epsilon}}$ and C_V are both independent of Reynolds number or if they both depend on Reynolds number in a way which cancels out when one takes the product $C_{\bar{\epsilon}}C_V$. To check that C_D is indeed independent of Re in our measurements , the plates were subjected to a range of velocities in the Donald Campbell tunnel, ranging between $5ms^{-1} \leq U_\infty \leq 20ms^{-1}$. A selection of the results can be seen in figure 6, although it should be noted that all the plates exhibited a Reynolds number independence for $Re > 1.5 \times 10^5$. The fact that the plates show a consistent trend in drag coefficient across a range of Reynolds numbers strengthens the support for our conclusions in section 3.1. Even at the lowest Reynolds number the difference between the largest and smallest force is 16 times larger than the resolution of the ATI sensor implying that the changes in drag coefficient that we observe are real effects, particularly at the higher Reynolds numbers.

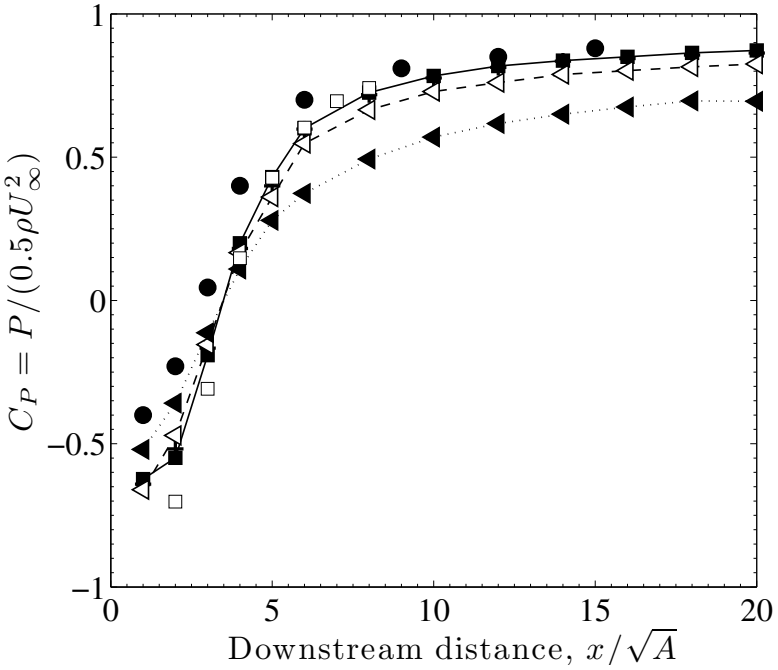

Figure 7. Axial pressure coefficient for the square (■), cross plate (+), $D_f = 1.3(4)$ (◁) and $D_f = 1.5(4)$ plate (◀) in the Honda tunnel. The figure also shows the data collected by Carmody [3] for the circular disk (•) as well as data for the square plate and $D_f = 1.5(4)$ plate in the DC Tunnel (□). Lines added to data points to show difference between data sets

4. Near wake measurements

Whilst measurements could be taken up to $x = 20\sqrt{A}$ downstream of the plate in the Honda tunnel, the relatively short length of the test section compared to the size of the plate in the DC Tunnel meant that measurements could only be taken for the first eight characteristic lengths. It is in the Honda tunnel that the main bulk of axial measurements are taken, whilst planar measurements were taken in the DC Tunnel.

4.1. Axial pressure and turbulence measurements

Using a Pitot-static probe, the axial pressure i.e. along the x-direction on the centre-line crossing the centre of the plate, was collected for all the plates from $x = \sqrt{A}$ to $x = 20\sqrt{A}$ in the Honda Tunnel. Our results, along with those of [3] for the circular disk, are shown in figure 7, where the coefficient of pressure is defined as $C_P = P/(0.5\rho U_\infty^2)$, with P being the dynamic pressure (i.e. total pressure minus static pressure) of the Pitot-static tube in the wake of the plates. Based on these results, it would appear that there is little difference between the square and the cross plate and that even the $D_f = 1.3(4)$ has similar pressure coefficient values. The $D_f = 1.5(4)$ however shows a smaller pressure drop close to the plate and a very slow rate of pressure recovery; even at a distance of $20\sqrt{A}$ the wake has not recovered to the same levels as the other

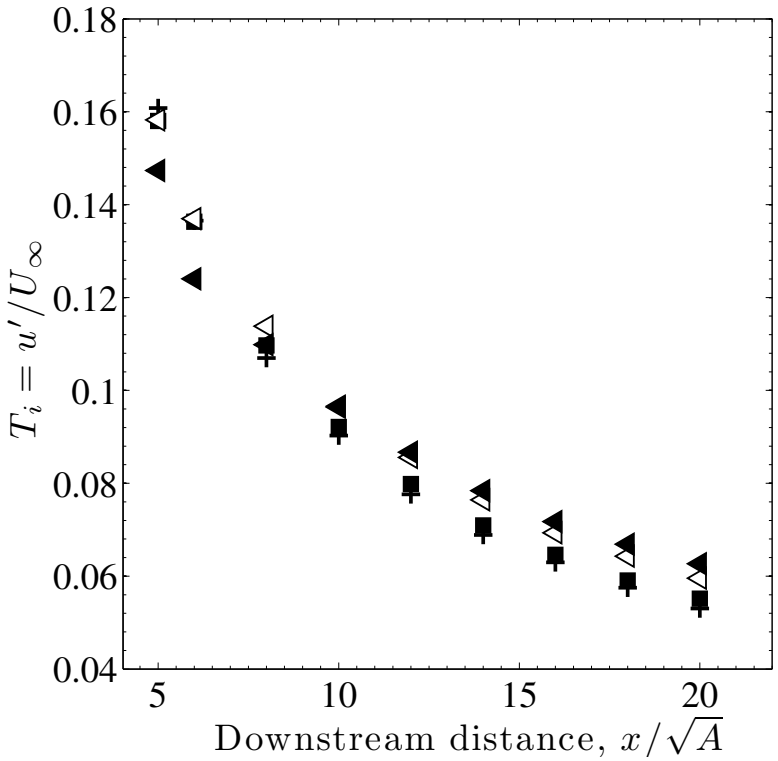

Figure 8. Axial turbulence intensity measurements for the square (■), cross plate (+), $D_f = 1.3(4)$ (◁) and $D_f = 1.5(4)$ plate (◀), data collected in the Honda tunnel.

plates. Although only the fourth iteration of both fractal dimension families are shown, it should be noted that there is a decreasing pressure drop behind the plate for increasing fractal iteration and that further downstream there is a faster rate of pressure recovery as fractal iteration is increased. These results also suggest, judging from the position where $C_P = 0$, that the length of the re-circulating region is roughly similar for all plates, however, no conclusions can be made about the overall volume of the bubble itself.

The axial evolution of the turbulence intensity, $T_i = u'/U_\infty$ where u' is the fluctuating velocity, is shown in figure 8 for the square, cross and the last iteration of both fractal plates where, just as before, there is no noticeable difference between the T_i values for the cross and square plates. Here we observe that at the closest position the fractal plates have lower levels of turbulence intensity compared to the square and cross plate, however after $x \geq 6\sqrt{A}$, there is a noticeable change where the fractal plates actually have higher levels of turbulence intensity, and at a distance of $x = 20\sqrt{A}$, the $D_f = 1.5(4)$ has the highest level of T_i of all the plates.

As in figure 7, figure 8 shows the fourth iteration of both fractal dimension families, which had the lowest turbulence intensity close to the plate and the highest further downstream compared to the other fractal iterations i.e. the rate of decay decreased as fractal dimension and iteration increased.

4.2. Planar measurements in the near wake

It is clear that although one could use the axial measurements for direct comparison from one plate to another, the same can not be said for a single traverse through the wake, as is often the practice with axisymmetric plates. Although the square and cross plate both have reflection and rotation symmetry, they are not axisymmetric and so one must take planar measurements to fully understand the development of the wake. This point is even more critical for the fractal plates which only have rotation symmetry (by 90°). Planar measurements of the pressure coefficient are taken in the DC Tunnel.

In equation (1), the wake volume coefficient as well as the dissipation coefficient are defined over all fluid space which is assumed to be infinite, however in practice it is not possible to measure these values over an infinite domain of the wake. The volume coefficient in equation 1 can however be decomposed into the sum of 2D normal slices through the wake over several downstream locations, that is to say $C_V = A^{-1.5}\int_0^\infty C_A dx$, where C_A is now defined as:

$$C_A = \frac{A_{wake}}{A} \tag{7}$$

where A_{wake} is the planar, cross-section area of the wake and is the only variable that is a function of x. This area can be approached experimentally in a number of ways, however for this study we shall define a length based on a certain fraction of the velocity deficit, U_d in the wake, where the velocity deficit is defined as $U_d = U_\infty - < U(x,y,z) >$ and the corresponding length is the point where the deficit velocity is some fraction, ζ, of the centre-line velocity deficit, that is to say $U_d(x, \pm y_\zeta, \pm z_\zeta) = \zeta U_d(x,0,0)$ (U is the streamwise velocity component of the fluid velocity and the brackets $< ... >$ signify an average over time). As we are collecting pressure from the rake measurements, this can also be expressed as:

$$1 - \sqrt{C_P(x, \pm y_\zeta, \pm z_\zeta)} = \zeta(1 - \sqrt{C_P(x,0,0)}) \tag{8}$$

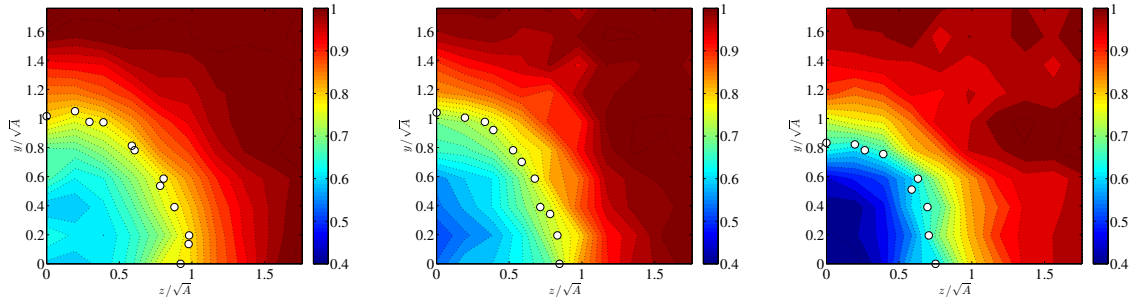

(a) Square (b) $D_f = 1.3(4)$ (c) $D_f = 1.5(4)$

Figure 9. Contour plots of C_P at a distance of $x = 6\sqrt{A}$ downstream of the plates, including small circles which are the calculated wake boundary based on $\zeta = 0.5$

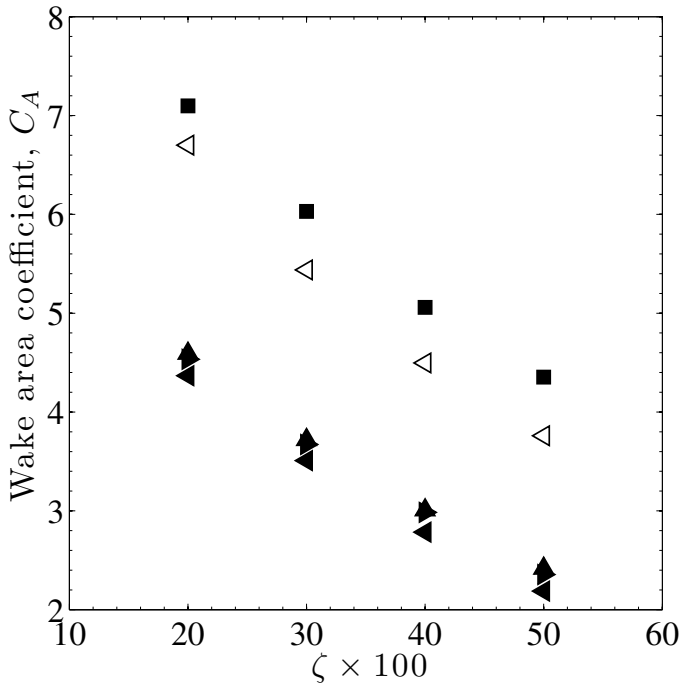

Figure 10. Coefficient of area, C_A as determined from various values of ζ taken at a distance x = $6\sqrt{A}$ for: (■) - square, (◁) - D_f=1.3(4), (▲) - D_f = 1.5(1), (►) - D_f = 1.5(2), (◄) - D_f = 1.5(4)

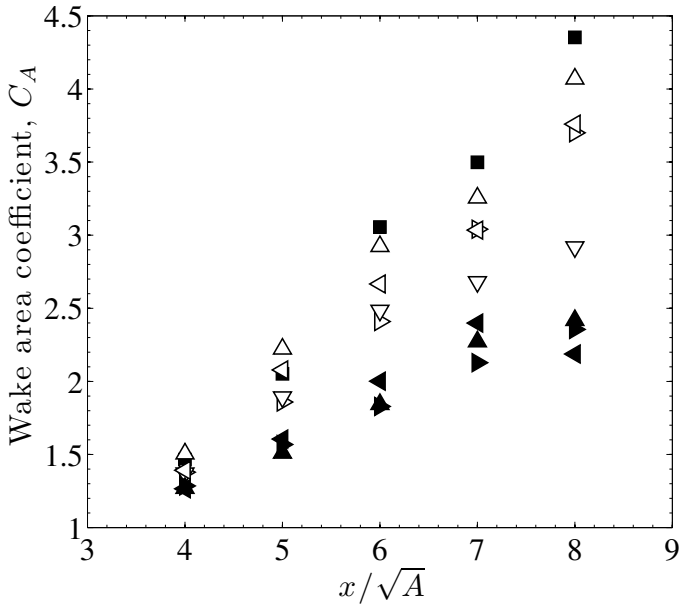

Figure 11. Downstream evolution of the coefficient of area, based on $\zeta = 0.5$ for all the plates, where: (■) - square, (△) - D_f=1.3(1), (▷) - D_f=1.3(2), (▽) - D_f=1.3(3), (◁) - D_f=1.3(4), (▲) - D_f = 1.5(1), (►) - D_f = 1.5(2), (◄) - D_f = 1.5(4)

The value of the width was found by fitting a sixth order polynomial to the data and finding the point where the velocity deficit was a certain fraction ζ, of the centre-line deficit velocity. Note that y_ζ and z_ζ are the vertical and spanwise distances from the centreline (see figure 2 for definition), where the pressure coefficient is a certain fraction ζ of the centreline pressure coefficient. Finally to obtain an estimate of the wake area, the area in plots such as those in figure 9 was integrated from the origin to newly created data points identified as the white circles in that figure.

As already mentioned in Section 2, the spacing between the Pitot probes on the rake was set to 50mm, however to determine whether this spacing was adequate to obtain the area of the wake a preliminary test was done. At a distance of $x = 6\sqrt{A}$ the rake was traversed by 10mm in the z direction (see figure 2 for definition of coordinates) thus obtaining 40 data points which were 10mm apart. The width of the wake was found in the same way as described above for both sets of data i.e. one with 10 data points and another with 40 data points, where it was found that both sets of data gave similar results. It is believed however that the accuracy of this method would be lower closer to the plate where the wake is much smaller and hence there are less data points available for the polynomial fit. Similarly, this method does not work when there are negative C_P values, which is why we show data from $x = 4\sqrt{A}$ onwards.

In figure 9 we show the planar pressure coefficient measurements taken in one quarter of the wake for a selection of plates, where the corresponding co-ordinates of the detected wake edge can also be seen. These boundaries are based on a ζ value of 0.5, i.e. the point where the pressure reaches 50% of the centre-line pressure. From a quick inspection, it appears that the wake of the $D_f = 1.5(4)$ is the smallest of all the plates - see figure 9(c) and that, just as was noted in figure 7, it has a very low pressure coefficient in the middle of the wake. We have, for simple comparison, also plotted in figure 7 the centre-line evolution of the pressure coefficient of the square plate taken in the DC Tunnel where good agreement between the two tunnels is observed.

As mentioned earlier a number of values for ζ were looked at, and it was observed that the trend of C_A from one plate to another was always consistent irrespective of the value of ζ, as can be seen in figure 10. This does suggest that most of the information in terms of getting a good value for C_A can actually be obtained from looking at the point where the pressure reaches 50% of the centre-line pressure. From these results, the impression seems to be that no matter what value of ζ is chosen, the area of wake for the square plate will be the largest, followed by the $D_f = 1.3$ family of plates, although only the last iteration is shown here for clarity. The smallest wake can be seen for the $D_f = 1.5$ family of plates, but it must be pointed out that these results are for one downstream location at $x = 8\sqrt{A}$.

If we now look at figure 11 where the growth of the wake is shown, we see a clear pattern emerging between the fractal dimensions at $x/\sqrt{A} \geq 6$, with all the $D_f = 1.3$ family of plates having a smaller coefficient of area for all positions compared to the square plate, but a larger C_A compared to the $D_f = 1.5$ fractal plates. This fact is particularly interesting because if we use the drag coefficients from the DC Tunnel,

where the planar measurements are taken, then we note that the square, the first three iterations of the $D_f = 1.3$ plates and the last iteration of the $D_f = 1.5$ plates all have similar drag coefficients, but the pressure in the wake and the size of the wake are very different in each case. This means that there must be, as predicted in Section 1.3, another effect causing the drag to stay the same even though the areas are different.

Figure 11 also shows an indication that the area coefficient changes with iteration, particularly for the $D_f = 1.3$ fractal plates where C_A drops for consecutive iterations before increasing again for the last iteration, particularly at the largest value of $x/\sqrt{A}$.

5. Flow shedding

The final aspect of the wake that we study is the flow shedding. From the literature, there appears to be no discernible difference in the Strouhal number ($St = f\sqrt{A}/U_\infty$ where f is the shedding frequency) for the various plates that have been studied, suggesting that the Strouhal number may be independent of the shape of the plate (with the one exception of the circular disk from [7]) generating the wake. By adding so many discontinuities and length-scales to the perimeter of the plate, it would be interesting to see if the shedding changes in any way.

With the single hot-wire probe located at a distance $x = 5\sqrt{A}$, measurements were taken at eight polar locations from $0° \leq \theta \leq 315°$, with a radius of 200mm from the axial line (see figure 2) as this position was found to have, on the whole, a stronger signal from the hot-wire for all the plates. It should also be noted that the turbulence intensity in this region was less than 15%. The radial results for the square plate and the $D_f = 1.5(4)$ fractal plate, taken at $x = 5\sqrt{A}$, are shown in figure 12 where it can be

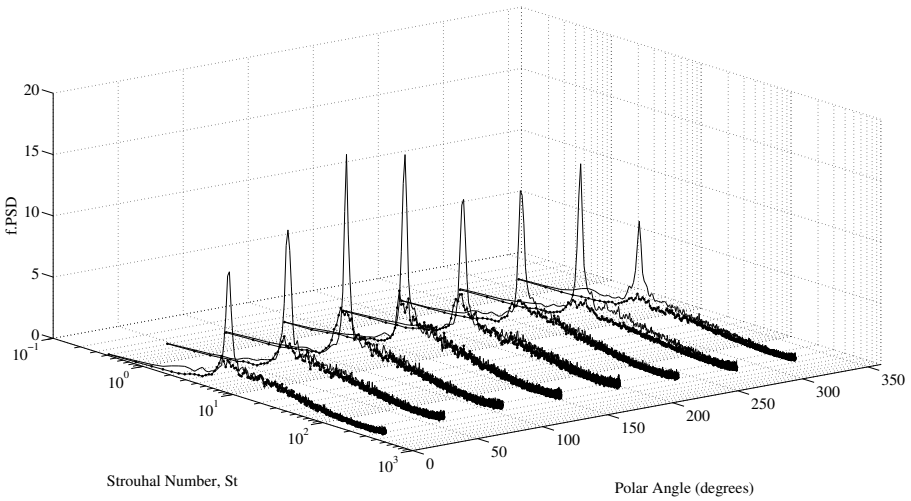

Figure 12. Power spectral density multiplied by f as a function of St at various polar angles for the square plate [——] and the $D_f = 1.5(4)$ fractal plate [●], taken at a distance of $x = 5\sqrt{A}$.

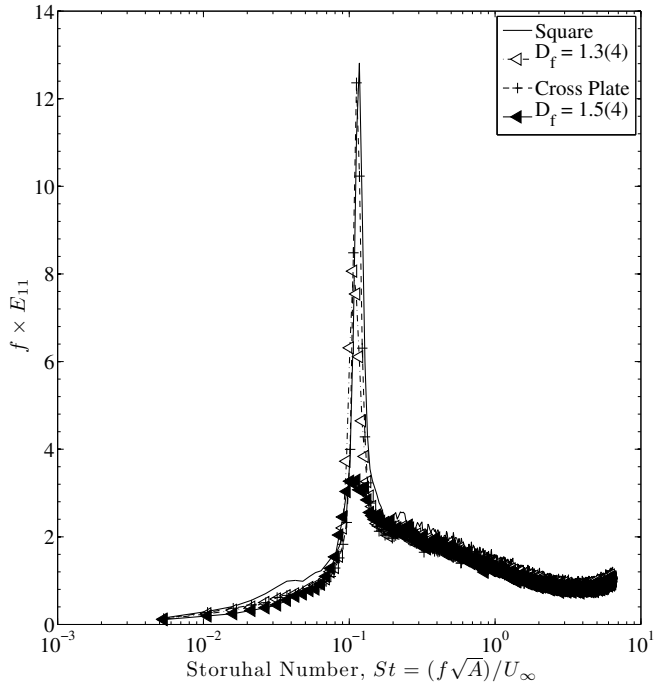

(a)

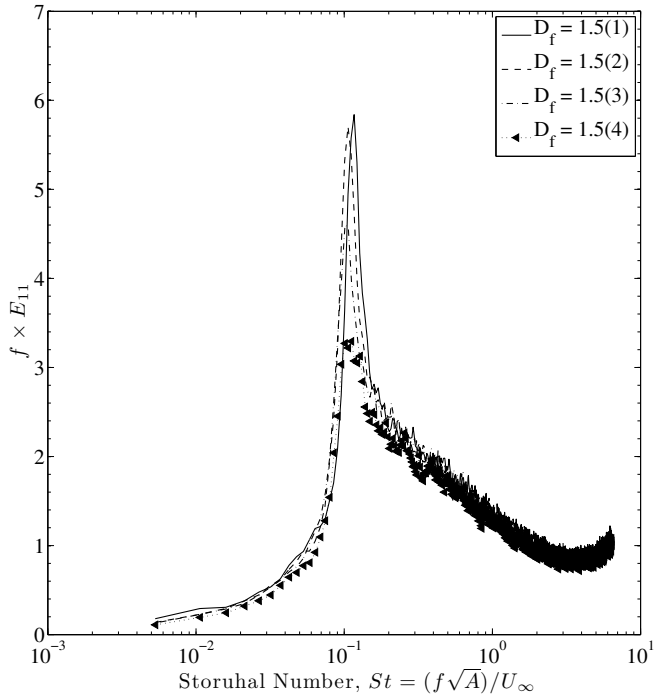

(b)

Figure 13. Mean pre-multiplied power spectral density for (a) a selection of plates and (b) for the $D_f = 1.5$ fractal plates at a distance of $x = 5\sqrt{A}$. Data collected in the Honda Tunnel.

seen that the power spectral density of the velocity fluctuations for the square plate are consistently higher than the $D_f = 1.5(4)$ plate, even though they all shed at the same Strouhal number. It was found that the Strouhal number ranges between 0.11-0.12 for all plates, which is in good agreement with previous studies.

The results therefore suggest that the impact of the fractal geometries on the perimeter of the plates is to diminish the intensity of the shedding from the plates, but not the rate at which the flow is shed off the plate. There is even an effect between consecutive iterations and fractal dimension, with the intensity of the shedding diminishing with increasing iteration and fractal dimension, as can be seen in figure 13 where the $D_f = 1.5(4)$ has the lowest amount of energy from all the plates by a factor of four compared to the square plate. Note that this is based on data for a single downstream and radial location. Fractal edges can therefore presumably be used on plates to very significantly reduce vibration. This aspect will be the object of a future study.

6. Conclusion

A non-negligible change in the drag coefficient of up to 7% is observed for flat plates with fractal edges placed normal to an incoming laminar flow. It is therefore possible to change the drag coefficient which was deemed to be insensitive to the shape of the plate's rim from previous studies. This significant change in drag coefficient is insensitive to Reynolds number, but does strongly depend on the fractal dimension, D_f, and fractal iteration n.

The energy balance between the work required to move a plate through a fluid and the rate of kinetic energy dissipation in the wake leads to the expression $C_D = C_V C_{\bar{\epsilon}}$ where C_V is a dimensionless volume of the wake and $C_{\bar{\epsilon}}$ is a dimensionless aggregate rate of turbulent dissipation. This equation suggests that the drag of a blunt object can be controlled by either changing the dissipation in the wake, or by keeping the dissipation constant but by somehow changing the shape of the wake or even a combination of the two. Fractal geometries were used here to create plates for which the volume of the wake can be modified without modifying the area of the plate. The wake becomes smaller as the fractal dimension and the fractal iteration are increased.

We also found that increasing the fractal dimension and iteration causes a reduction in the intensity of the shedding, although the frequency at which the flow is shedding does not change.

This paper is, in a sense, introductory and much effort needs now to be focused in future work on the dissipation properties of these wakes as well as their later sections, such as the intermediate and the far wake, where it is known that the axisymmetric wake becomes self-similar.

Acknowledgements

The authors would like to acknowledge Tianyi Han and Victoria White for the acquisition of additional force measurements in the Donald Campbell tunnel as part of their Masters projects.

References

[1] Fail R, Lawford J A and Eyre R C W 1957 *Low speed experiments on the wake characteristics of flat plates normal to an airstream* (Ministry of Aviation)
[2] Marshall D and Stanton T E 1931 *Proceedings of the Royal Society of London. Series A, Containing Papers of a Mathematical and Physical Character* **130** 295–301 ISSN 09501207 URL `http://www.jstor.org/stable/95531`
[3] Carmody T 1964 *Journal of Basic Engineering* **86** 869
[4] Bearman P W 1971 *Journal of Fluid Mechanics* **46** 177–198 ISSN 0022-1120
[5] Humphries W and Vincent J H 1976 *Journal of Fluid Mechanics* **75** 737–749 ISSN 0022-1120
[6] Humphries W and Vincent J H 1976 *Applied Scientific Research* **32** 649–669
[7] Berger E, Scholz D and Schumm M 1990 *Journal of Fluids and Structures* **4** 231–257
[8] Lee S J and Bearman P W 1992 *Journal of fluids and structures* **6** 437–450
[9] Miau J J, Leu T S, Liu T W and Chou J H 1997 *Experiments in fluids* **23** 225–233
[10] Kiya M, Ishikawa H and Sakamoto H 2001 *Journal of Wind Engineering and Industrial Aerodynamics* **89** 1219–1232
[11] Shenoy A and Kleinstreuer C 2008 *Journal of Fluid Mechanics* **605** ISSN 0022-1120
[12] Kiya M and Abe Y 1999 *Journal of fluids and structures* **13** 1041–1067
[13] Seoud R E and Vassilicos J C 2007 *Physics of Fluids* **19** 105108
[14] Laizet S and Vassilicos J 2012 *Physical Review E* **86** ISSN 1539-3755
[15] Kang H S, Dennis D and Meneveau C 2011 *Fractals* **19** 387–399 ISSN 0218-348X
[16] Gomes-Fernandes R, Ganapathisubramani B and Vassilicos J C 2012 *Journal of Fluid Mechanics* **711** 306–336 ISSN 0022-1120
[17] Abou El-Azm Aly A, Chong A, Nicolleau F and Beck S 2010 *Experimental Thermal and Fluid Science* **34** 104–111
[18] Nicolleau F, Salim S M M and Nowakowski A F 2011 *Journal of Turbulence*
[19] Mandelbrot B B 1983 *The fractal geometry of nature* (WH Freeman and Co., New York)

Appendix

The derivation of Equation 1

Consider a plate moving with constant speed U_∞ in a viscous fluid that is stationary at infinity. The work performed in moving the plate against the drag $D =< \int_{plate-surface} dS(-\mathbf{n}\cdot\mathbf{u}p + \nu\omega\times\mathbf{n}\cdot\mathbf{u}) >$, balances the dissipation rate of the kinetic energy of the fluid, $\int \rho\epsilon(\mathbf{x})dV$, where the volume integral is over all fluid-space (assumed infinite), the brackets $< \ldots >$ represent a time average and $\epsilon(\mathbf{x})$ is the time-averaged kinetic energy dissipation rate per unit mass, i.e. $\epsilon(\mathbf{x}) = \sum_{i=1}^{3}\sum_{j=1}^{3}\nu < (\partial u_i/\partial x_j)^2 >$. In this balance, we have neglected a surface integral term representing energy dissipation rate by surface friction, as skin friction drag is negligible for blunt objects such as plates normal to the flow.

The vast majority of the kinetic energy dissipation resides inside the turbulent wake and the volume, V_{wake}, of this wake can therefore be used to define an average dissipation by: $V_{wake}\bar{\epsilon} = \int \epsilon(\mathbf{x})dV$, where the integral is over the volume of the wake. We define the dissipation rate coefficient $C_{\bar{\epsilon}}$ as $\bar{\epsilon} = C_{\bar{\epsilon}}U_\infty^3/\ell$, where ℓ is a characteristic length of the object that is creating the wake, defined as $\ell = \sqrt{A}$ for our study. The balance between the work performed in moving the plate, which is DU_∞, and the dissipation rate $\int \rho\epsilon(\mathbf{x})dV$ leads to:

$$C_D = C_V C_{\bar{\epsilon}} \tag{9}$$

where the wake volume coefficient is defined as $C_V = V_{wake}/2A^{1.5}$ with A being the frontal area of the plate and the characteristic length ℓ being defined as $\sqrt{A}$. A similar relationship can be found for a planar wake, where equation 1 becomes $C_D = C_A C_{\bar{\epsilon}}$, with $C_A = A_{wake}/A$.